Article

Cell Reports

Divergent Expression and Metabolic Functions of Human Glucuronosyltransferases through Alternative Splicing

Graphical Abstract

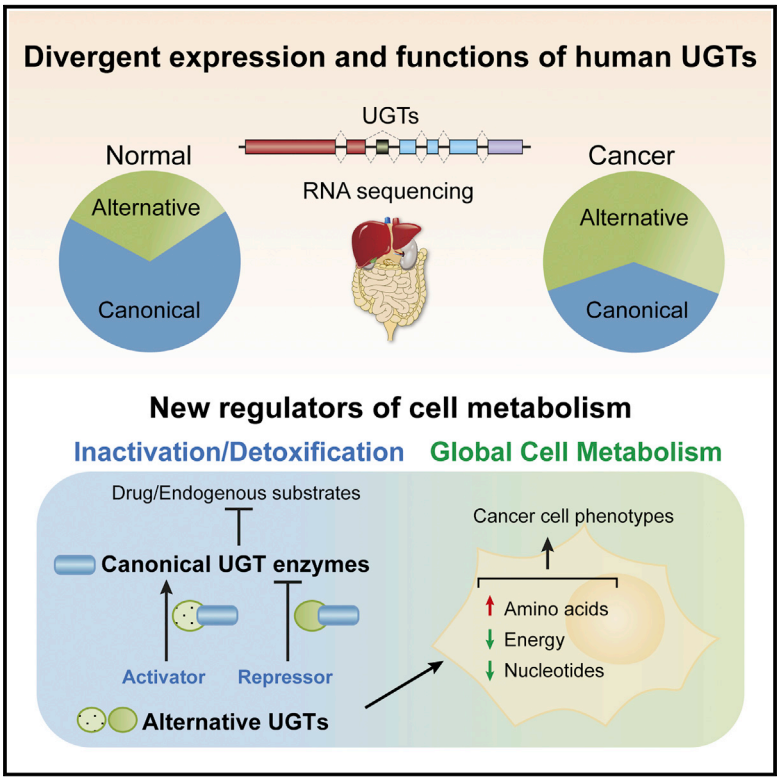

Highlights

- Alternative UGTs quantitatively represent 20%–60% of canonical transcripts
- 20% of these UGTs acquire sequences predicted to give distinct structural features
- Alternative UGTs with in-frame sequences modify cell detoxification activity
- These UGTs are linked to changes in metabolism and cellular phenotypes

Authors

Michèle Rouleau, Alan Tourancheau, Camille Girard-Bock, ..., Ion Popa, Arnaud Droit, Chantal Guillemette

Correspondence

chantal.guillemette@crchudequebec.ulaval.ca

In Brief

Rouleau et al. find that multiple alternative isoforms of the detoxification enzymes UDP-glucuronosyltransferases (UGTs) are highly expressed in metabolic tissues. They show that alternative UGTs regulate cell metabolism by modulating conjugation activity and inducing global metabolic reprogramming concurrent with altered cell adhesion and proliferation.

Accession Numbers

GSE80463

Rouleau et al., 2016, Cell Reports *17*, 114–124
September 27, 2016
http://dx.doi.org/10.1016/j.celrep.2016.08.077

OPEN ACCESS
CellPress

Cell Reports
Article

Divergent Expression and Metabolic Functions of Human Glucuronosyltransferases through Alternative Splicing

Michèle Rouleau,[1,2] Alan Tourancheau,[1,2] Camille Girard-Bock,[1,2] Lyne Villeneuve,[1,2] Jonathan Vaucher,[3] Anne-Marie Duperré,[1,2] Yannick Audet-Delage,[1,2] Isabelle Gilbert,[1,2] Ion Popa,[3] Arnaud Droit,[3] and Chantal Guillemette[1,2,4,*]

[1]Pharmacogenomics Laboratory, Centre Hospitalier Universitaire de Québec Research Center, Québec, QC G1V 4G2, Canada
[2]Faculty of Pharmacy, Laval University, Québec, QC G1V 0A6, Canada
[3]Faculty of Medicine, Laval University, Québec, QC G1V 0A6, Canada
[4]Lead Contact
*Correspondence: chantal.guillemette@crchudequebec.ulaval.ca
http://dx.doi.org/10.1016/j.celrep.2016.08.077

SUMMARY

Maintenance of cellular homeostasis and xenobiotic detoxification is mediated by 19 human UDP-glucuronosyltransferase enzymes (UGTs) encoded by ten genes that comprise the glucuronidation pathway. Deep RNA sequencing of major metabolic organs exposes a substantial expansion of the UGT transcriptome by alternative splicing, with variants representing 20% to 60% of canonical transcript expression. Nearly a fifth of expressed variants comprise in-frame sequences that may create distinct structural and functional features. Follow-up cell-based assays reveal biological functions for these alternative UGT proteins. Some isoforms were found to inhibit or induce inactivation of drugs and steroids in addition to perturbing global cell metabolism (energy, amino acids, nucleotides), cell adhesion, and proliferation. This work highlights the biological relevance of alternative UGT expression, which we propose increases protein diversity through the evolution of metabolic regulators from specific enzymes.

INTRODUCTION

Human glycosyltransferases utilize different sugar nucleotide donors to regulate a wide variety of cellular processes (Breton et al., 2012; De Bruyn et al., 2015; Guillemette et al., 2004; Little et al., 2004; Rowland et al., 2013). One large family of membrane-associated uridine diphospho-glucuronosyltransferases (UGTs) employs uridine diphospho-glucuronic acid (UDPGA) to conjugate a variety of small-molecule acceptors and catalyze the most important metabolic pathway for the human body's elimination of both endogenous and exogenous lipophilic molecules. These ER resident type I membrane proteins transfer the sugar moiety of the co-substrate UDPGA to the nucleophilic functional group of their substrates to promote, in most cases, their inactivation and elimination. Glucuronidation affects the bioactivity and bioavailability of harmful xenobiotics, chemicals, and drugs from food, the environment, or pharmacological treatments. In parallel, glucuronidation maintains the homeostasis of the heme breakdown product bilirubin, multiple endogenous hormones, secondary metabolites, and other endobiotics (Bock, 2015; Guillemette, 2003; Radominska-Pandya et al., 1999; Wells et al., 2004).

In humans, ten genes encode 19 canonical UGT enzymes (isoform 1s [i1s]) that display remarkable plasticity. For example, a single *UGT1* gene on chromosome 2q37 encodes nine UGT1A enzymes through usage of individual alternative promoters and first exons, whereas ten UGT2 enzymes (three UGT2A and seven UGT2B enzymes) are synthesized from nine independent genes clustered on chromosome 4q13 (Mackenzie et al., 2005). Although amino acid sequences among UGTs are highly similar, substrate specificity is dictated by the slightly more divergent first (UGT1) or first/second (UGT2) exons that encode the N-terminal half of each enzyme. UGTs are found in nearly all human tissues and display tissue- and cell-type-specific expression, but they are most abundant in metabolically highly active organs such as the liver, kidney, and intestine (Court et al., 2012; Margaillan et al., 2015a, 2015b; Rowland et al., 2013).

Alternative splicing (AS) is a key mechanism in the control of gene expression, transcriptomes, and protein diversity, with over 90% of human multi-exon genes undergoing AS regulation before forming mature transcript isoforms (Wang et al., 2008). The important contributions of AS to an individual's response to endogenous and exogenous molecules, including drugs, and the link to various human diseases are emerging but remain largely unknown (Gamazon and Stranger, 2014; Garcia-Blanco et al., 2004; Oltean and Bates, 2014). Our recent work established that AS expands the coding capacity of human *UGT*s, allowing over 180 canonical and alternative *UGT* transcripts in various tissues involved in drug metabolism as well as hormone-dependent tissues (Tourancheau et al., 2016). Thus, a large genetic diversity characterizes the transcriptome landscape of human *UGT*s and implies a functional diversification of the UGT proteome that remains unexplored.

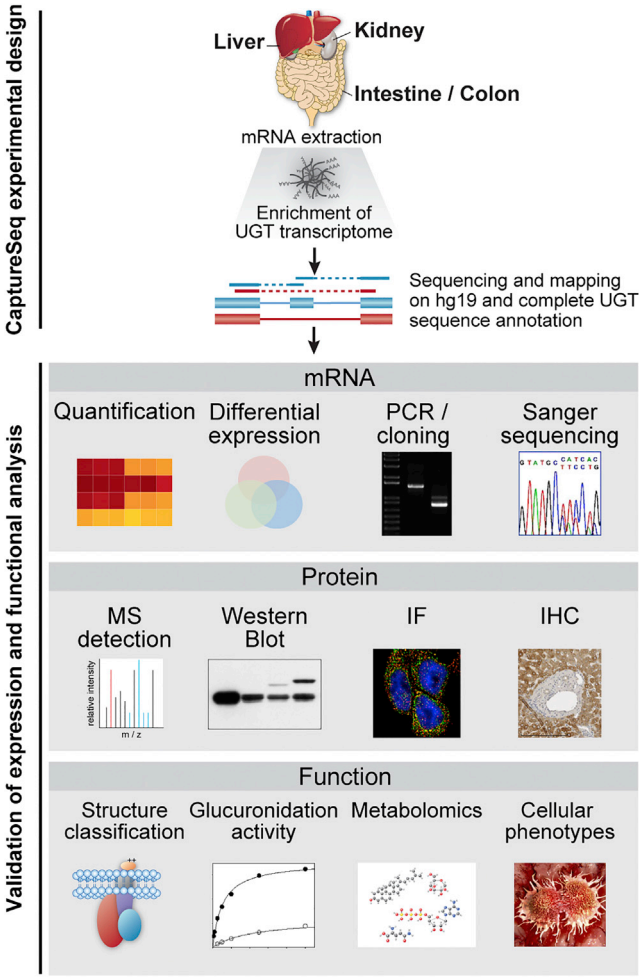

Figure 1. Profiling the UGT Transcriptome and Characterization of UGT Isoforms: An Overview of the Experimental Design

The UGT transcriptome in the main drug metabolizing organs (nine or more samples per tissue) was quantified by RNA-seq after a targeted capture step. The complete human UGT sequence annotation (Tourancheau et al., 2016) enabled precise mapping of reads to canonical and alternative transcripts. Expression and functional analysis of mRNA variants and predicted protein isoforms were conducted by multiple approaches.

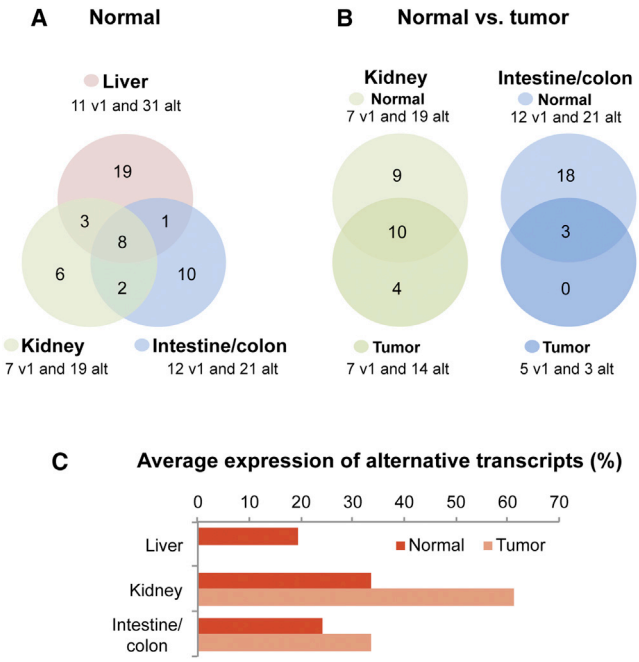

Figure 2. Tissue-Specific Expression of Canonical and Alternative *UGT* Transcripts

(A and B) Venn diagrams showing the large diversity in expression patterns between tissues (A) and between healthy and tumor tissues (B). The total numbers of canonical (v1) UGTs and alternative variants (alt) are given for each tissue. The values in the Venn diagrams represent the number of alternative transcripts (alt) expressed above 600 fragments per kilobase of transcript per million mapped reads in CaptureSeq.

(C) Average quantitative expression of alternative transcripts in healthy and tumor tissues. Total expression of alternative transcripts relative to total v1 expression in each tissue is represented.

See also Figure S1.

In this study, we applied targeted next-generation RNA sequencing (CaptureSeq) (Clark et al., 2015; Mercer et al., 2011) to quantify the UGT transcriptome and expression of alternative transcripts in the liver, kidney, and gastrointestinal tissues, which are most relevant to the metabolic functions of this crucial enzymatic pathway. We further addressed tissue-specific protein expression as well as the function of selected UGT isoforms where in-frame sequences have been introduced using cell-based assays combined with untargeted metabolomics (Figure 1). Our findings reveal a complex expression pattern of UGT alternative variants and distinct functional properties, including antagonizing and inducing UGT transferase function, likely through protein-protein interaction, while inducing substantial rewiring of cell metabolism that affects cellular behavior.

RESULTS

AS Contributes to Quantitative Profiles of the UGT Transcriptome in Human Metabolic Tissues

A quantitative transcriptome analysis of all ten human *UGT1* and *UGT2* genes was conducted in pooled samples of normal liver, kidney, and intestine/colon tissues as well as in tumors originating from the kidney and the intestine/colon. A CaptureSeq approach was used to achieve sufficient sequencing depth and ensure the fullest coverage of alternative UGT variants. Reads were mapped to the human genome sequence (hg19) complemented with the recently published comprehensive human UGT transcriptome (Tourancheau et al., 2016; Figure 1). The data revealed that AS contributes substantially to the UGT transcriptome landscape, affecting each expressed *UGT1* and *UGT2* gene in a tissue-specific manner, and the AS products are significantly altered in neoplastic tissues (Figures 2A and 2B). Alternatively spliced species were abundant in normal tissues, representing an average of 19%, 24%, and 34% of the total UGT expression in the liver, intestine/colon, and kidney, respectively (Figure 2C). In intestine/colon and kidney tumor tissues, these levels were strikingly elevated to an average of

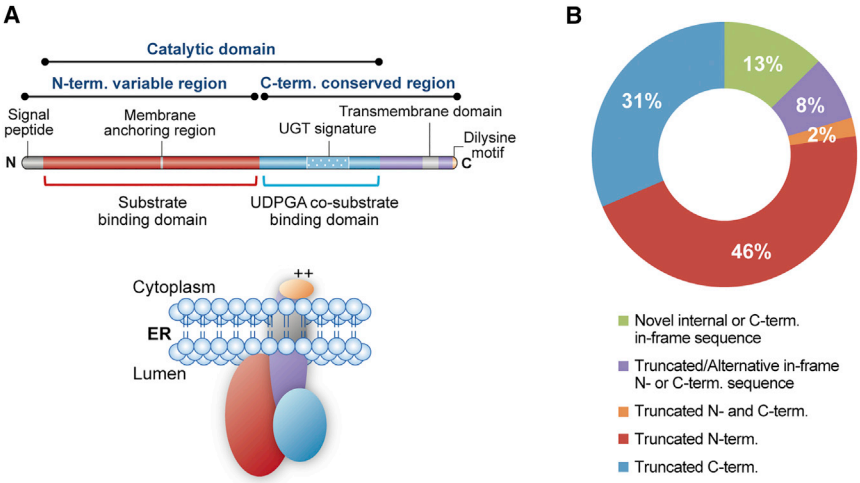

Figure 3. Structural Organization of UGT Enzymes and Alternative Isoforms

(A) Schematic of functional domains and structural organization of UGT enzymes in the ER. The bulk of the substrate-binding (red) and co-substrate-binding (blue) domains lies on the luminal side of the ER. The transmembrane domain (gray segment) positions the positively charged tail (orange, ++) on the cytoplasmic side of the ER. N-term, N-terminal; C-term, C-terminal.

(B) Relative quantification of alternative UGT levels classified on the basis of truncated regions and inclusion of sequences predicted from alternative transcript expression levels.

33% and 61%, respectively. Changes in liver cancer could not be assessed because of the lack of availability of hepatic tumors. The abundance and tissue-specific expression of several alternative transcripts supports a physiologically relevant role in the surveyed tissues.

Diverse Structural Features of Alternative UGT Isoforms

A common structural organization is shared by the 19 known human UGT1 and UGT2 enzymes, each encoded by a canonical mRNA variant, v1. An N-terminal signal peptide and a C-terminal transmembrane region direct the substrate and UDPGA co-substrate-binding domains and catalytic site of each mature protein to the luminal side of the ER (Figure 3A). Based on these structural features, 164 expressed non-v1 alternative transcripts were classified into five categories (Figure 3B). Nearly half of the expressed alternative UGT variants lacked a sequence encoding the substrate-binding domain (N-terminal), frequently because of truncation or skipping of exon 1, and this alteration was especially frequent among *UGT2* transcripts. In the absence of the N-terminal substrate-binding domain, the encoded proteins would be expected to lack transferase activity. Another prominently expressed class of variants that constituted over one-third of alternative variants lacked part or all of the exons encoding the C-terminal co-substrate domain. Remarkably, over 20% of the expressed variants comprised introduction of in-frame sequences. The domain organization and sequences of the putative isoforms imply that several may have different subcellular distribution, substrate specificity, or catalytic activity and thus could have altered biological functions.

Functional Diversity of Selected Alternate UGTs Containing In-Frame Sequences

Shorter UGT1 Isoforms with an Alternative C-terminal Sequence Have Antagonistic Functions

A single *UGT1* locus encodes half of the human UGT enzymes; i.e., nine UGT1A enzymes. It is well established that mature transcripts encoding each UGT1A enzyme include only one of the different *UGT1* exon 1 sequences associated with four downstream exons common to all UGT1A enzymes (i1s). A splicing event involving the use of an alternative 3′-terminal exon (exon 5b) generates three categories of *UGT1* transcripts, namely the canonical *v1* (exon 5a) and alternative *v2* (exon 5b) and *v3* (exons 5b and 5a) (Figure 4A). Our CaptureSeq data and those of an independent RNA sequencing (RNA-seq) study revealed significant expression of *v2/v3*, with these transcripts representing between 9% and 20% of canonical *UGT1A* transcripts in normal tissues and high interindividual variability (Figures S1A and S1B). In kidney and intestine/colon tumor tissues, v2/v3 constituted between 19% and 23% of *UGT1A_v1* expression. Because of a stop codon in exon 5b, the alternative *v2/v3* variants both encode shorter, 45-kDa isoform 2 proteins (i2s) lacking the C-terminal 99 amino acid residues encoded by exon 5a that comprise the membrane-spanning domain and the short cytosolic charged tail. In alternate UGT1A_i2 proteins, this sequence is replaced by a charged ten-residue C-terminal sequence not found in any other human proteins. The functions of i2s were studied in the HEK293 human embryonic kidney cell line, in which endogenous UGTs are not detected. UGT1A1_i2 had a remarkably long half-life compared with that of UGT1A1_i1 (11.6 hr versus 1.3 hr), whereas co-expression of the two isoforms did not alter their respective half-lives (Figure 4B). In situ enzymatic assays in intact cells supported the notion that UGT1A1_i2 lacks transferase activity; rather, it has an antagonist role leading to a significant reduction in UGT1A1_i1-mediated glucuronidation of the anti-cancer agent SN-38 (the active metabolite of irinotecan, −73.5%, $p < 0.001$) and the endogenous substrate estradiol (E_2, −75%, $p < 0.001$) (Figure 4C). These antagonistic effects of i2 are consistent with the co-immunoprecipitation (IP) of UGT1A_i2 with UGT1A_i1 (Figure 4D) as well as with the co-localization of both isoforms in the ER as assessed by immunofluorescence (IF; Figure 4E) and in cells of human tissues by immunohistochemistry (IHC; Figure 4F). The data also indicated that UGT1A proteins are distributed in other subcellular compartments (Figure S2). In colon tissues, i1 and i2 co-localized at surface epithelial cells and in intestinal gland (crypt) cells, whereas in liver tissues, the two isoforms co-localized in hepatocytes.

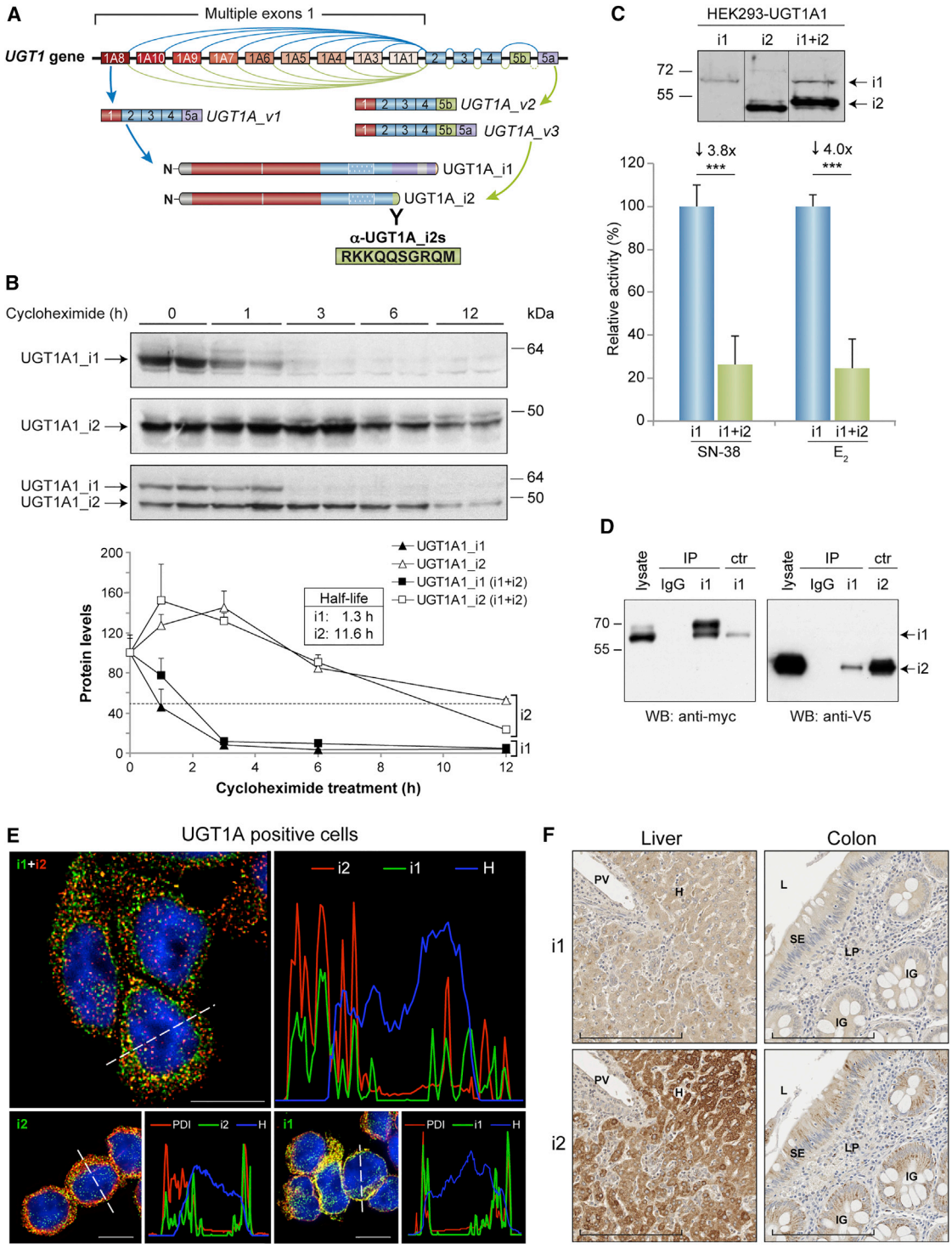

Figure 4. Functional Characterization of Alternate UGT1A_i2

(A) The nine well characterized UGT1A_v1 transcripts are produced from splicing of alternative exons 1 to the common exons 2–5a (blue lines) at the single *UGT1* locus and encode the nine UGT1A_i1 enzymes. The *UGT1A_v2* and *UGT1A_v3* transcripts (nine of each type) arise from the use of alternative exon 5b without or with exon 5a, respectively (green lines). *UGT1A_v2* and *_v3* transcripts encode the same nine UGT1A_i2 proteins because exon 5b includes a stop codon. UGT1A_i2 and UGT1A_i1 are distinguishable by their divergent C termini. The UGT1A_i2-specific antibody is directed toward the unique i2 amino acid sequence (green box). The domains are organized as in Figure 3A.

(legend continued on next page)

A UGT2B7 Isoform with a Spacer Domain Enhances Drug Inactivation and Provokes Remodeling of Cellular Metabolism and Phenotypic Changes

An alternative full-length *UGT2B7_n4* transcript, confirmed by PCR analysis as containing an introduced sequence, exon 2b (Figure S3A), encodes an alternate UGT2B7 protein termed isoform 8 (UGT2B7_i8) that has a unique 32-residue in-frame internal region residing at the interface between the N-terminal substrate-binding domain and the C-terminal co-substrate–binding domain (Figure 5A). CaptureSeq data analysis revealed that expression of exon 2b-containing transcripts in three pools of three liver samples was low compared with the canonical transcript (Figure S1C). However, the analysis of an independent RNA-seq dataset derived from 18 different individuals indicated that the UGT2B7_i8-encoding transcript represented up to 75% of the canonical UGT2B7 transcripts with an average coefficient of variation of 350% (Figure S1D). Similar patterns of expression were noted in the kidney, with a greater proportion of UGT2B7_i8-encoding transcript in kidney tumors relative to the canonical transcript. The encoded UGT2B7_i8 had a significant half-life of ~6 hr that was not affected when co-expressed with the i1 protein, which has a half-life of 12 hr (Figure S3B). Expression of the encoded i8 protein along with UGT2B7 in human liver was further established in hepatocytes using an i8-specific antibody, supporting the expression data of the alternative isoform and its partial co-localization with UGT2B7_i1 (Figure 5B). Staining was also observed in smooth muscle cells of hepatic arteries as well as in the same structures of esophageal, breast, uterine, testicular, and skeletal muscle tissues (data not shown), suggesting a potential unique cell type-specific expression of UGT2B7_i8 that deserves further investigation. Endogenous alternate protein expression was also corroborated by the detection of peptides specific to the sequence encoded by exon 2b in human liver samples using a targeted mass spectrometry (MS) approach (Figure S4).

UGT-negative (HEK293) and UGT-positive (HepG2) cell models were established to study the cellular functions of this UGT2B7 isoform and to reproduce the expression observed in tissues (i8 < i1). We could not detect the formation of glucuronide from zidovudine (AZT), the probe substrate of the UGT2B7 enzyme, in UGT2B7_i8-expressing HEK293 cells. However, the co-expression of UGT2B7_i8 and UGT2B7_i1 induced 1.3- and 2.1-fold increases in the formation of the glucuronide in HEK293 and HepG2 cells, respectively, implying a UGT-activating function (Figure 5C). The potential of UGT2B7_i8 and UGT2B7_i1 proteins to interact was further supported by co-IP experiments and by their co-localization in the ER and may underlie the induction in glucuronidation activity (Figures 5D and 5E). Untargeted metabolic profiling of the HEK293 and HepG2 cell models further revealed that the levels of a vast array of cellular metabolites were significantly altered in cells overexpressing UGT2B7_i8 compared with control cells (Figure 5F; Table S1). Despite the distinctive basal metabolomes of the kidney and liver cell models, expression of UGT2B7_i8 induced a remarkable accumulation of multiple amino acids in both cell types, with the glutamine level being most altered. Most purines and pyrimidines were reduced upon i8 expression in HEK cells, whereas several glycolytic and tricarboxylic acid (TCA) cycle intermediates were significantly reduced in HepG2 cells (Figure 5F; Table S1). These alterations in numerous metabolites essential for cell growth were associated with 3.5-fold enhanced adhesion but 3.7-fold slower proliferation in HEK293 cells overexpressing UGT2B7_i8 compared with control cells (Figure 5G). In support of a specific effect of the UGT2B7_i8 protein, the adhesion and proliferation of HEK293 cells overexpressing UGT2B7_i1 were similar to the control cells despite higher expression of i1 than i8.

DISCUSSION

Our findings reveal large differences in the levels of naturally occurring alternative mRNAs transcribed from *UGT* loci in major metabolic tissues and demonstrate that these alternate transcripts are expressed in a tissue-specific manner with remodeling of the UGT transcriptome in cancer tissues. Among this large collection of alternative UGT variants, expression of selected alternately spliced isoforms with in-frame sequences was confirmed at the protein level in human tissues such as the liver and colon. In cell-based assays, alternate UGT proteins were shown to differentially regulate the glucuronidation pathway by inhibiting or promoting the inactivation of drugs and hormones, likely through protein-protein interactions. We also uncovered that the alternate UGT isoforms have functions distinct from the canonical glucuronidation function, and these appear to broadly affect global metabolism, which results in changes in cell behavior. These findings imply that this transcriptome diversity expands the proteome and biological functions of human UGTs, likely playing crucial roles in multiple cellular processes.

Our targeted CaptureSeq approach allowed high-resolution quantitative evaluation of *UGT* expression in the liver, kidney, and intestine/colon. A strength of our study is the mapping of

(B) UGT1A_i2s have a longer protein half-life compared with UGT1A_i1. Top: protein levels of UGT1A1_i1, UGT1A1_i2, or both in the HEK293 cell models were measured at different times after treatment with cycloheximide using a pan-UGT1A antibody recognizing both isoforms. Bottom: densitometric quantification of the UGT1A protein level is expressed as a function of time after cycloheximide treatment. Data are presented as mean + SD.

(C) The HEK293 cell models (UGT-negative) were developed to express UGT1A1_i1, UGT1A1_i2, or both isoforms. In situ cell assays demonstrate that glucuronidation of SN-38 and E_2 by UGT1A1_i1 is impaired by the co-expression of UGT1A1_i2 (n = 2 independent assays in triplicate). UGT1A1_i2 did not catalyze glucuronidation of these substrates. Activity is normalized to the UGT1A1_i1 level. Data are presented as mean + SD. ***$p < 0.001$, Student's t test.

(D) Interactions between UGT1A_i1 and i2. IP of i1 from HEK cell lysates with the specific anti-i1 co-purifies UGT1A_i2. Lanes marked "ctr" served as markers for i1 and i2 protein mobility and detection.

(E) Endogenous UGT1A_i1 and i2 co-localize in the ER of colorectal cancer HT115 cells. PDI is an ER marker, whereas Hoechst (H) labels nuclei. Fluorescence intensity profiles are given for cross-sections (dashed lines). See also Figure S2 for a comparison of co-localization with multiple specific subcellular markers, including the ER. Scale bars, 10 μm.

(F) Immunohistochemical investigation of UGT1A_i1 and i2 in consecutive sections of normal human liver and colon tissues. H, hepatocytes; PV, portal vein; IG, intestinal gland; L, lumen; LP, lamina propria; SE, surface epithelium. Scale bars, 200 μm.

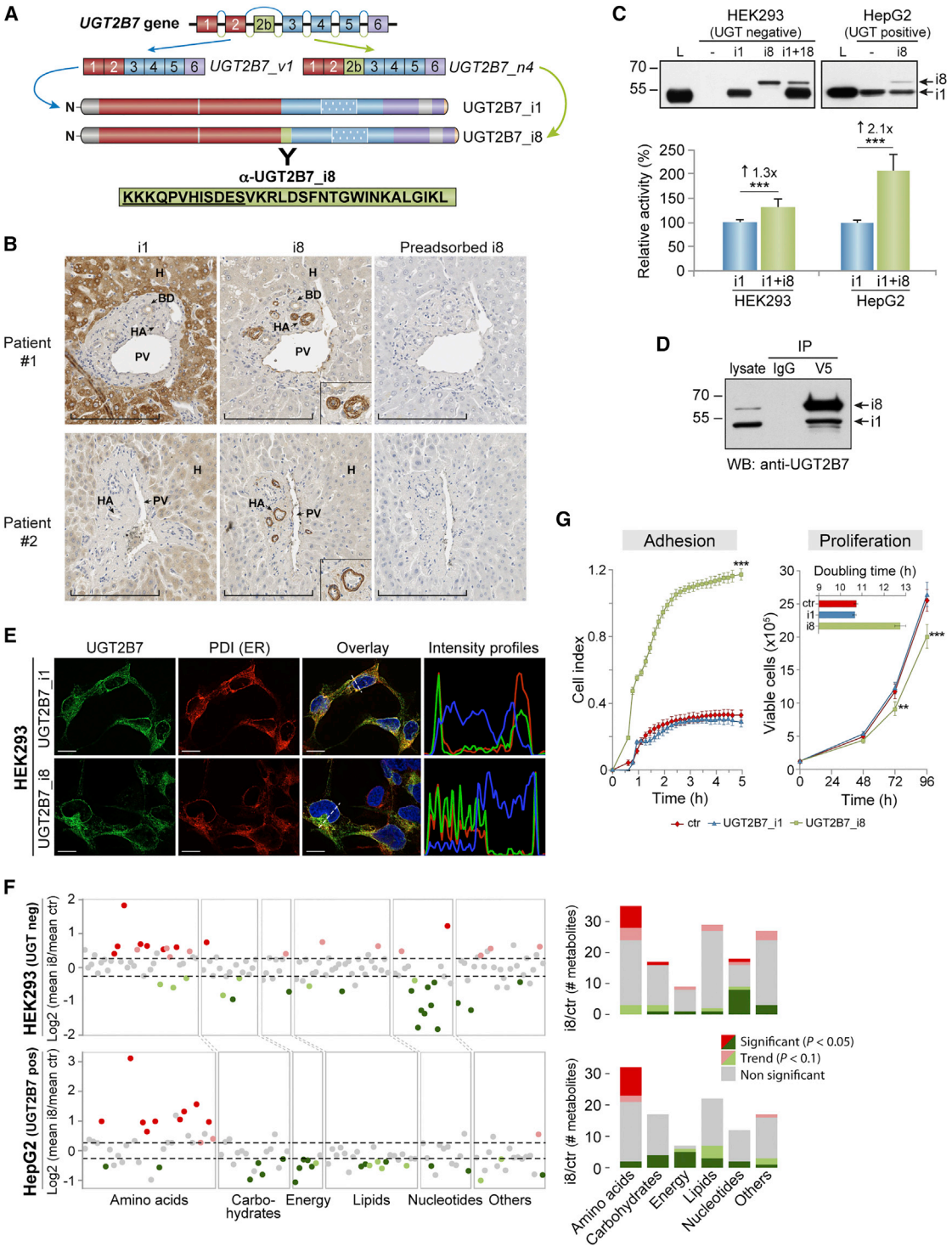

Figure 5. Functional Characterization of UGT2B7_i8

(A) Alternative splicing at the *UGT2B7* locus. The canonical *UGT2B7_v1* transcript excludes exon 2b (blue lines) and encodes the UGT2B7_i1 enzyme, whereas *UGT2B7_n4* includes exon 2b (green region, line, and boxed sequence) that extends the coding sequence to produce UGT2B7_i8. Anti-2B7_i8 was raised against the underlined immunogenic peptide.

(B) Immunohistochemical investigation of i8 expression in normal liver tissues. Left: UGT2B7_i1, labeled by the commercial antibody against UGT2B7, is expressed predominantly in hepatocytes but not in hepatic arteries or bile ducts. Center: the purified anti-i8 specifically and strongly labels smooth muscle cells of hepatic arteries, whereas hepatocytes are weakly labeled, and bile ducts are unlabeled. Right: labeling is impaired by preadsorption of anti-2B7_i8 with the

(legend continued on next page)

RNA sequencing short reads on the exhaustive human *UGT* transcriptome established recently (Tourancheau et al., 2016), leading to a more precise assignment of reads to the appropriate *UGT* loci and transcript reconstruction than previously possible. This work revealed that alternative *UGT* mRNAs constitute an appreciable proportion of the total UGT transcriptome in the surveyed tissues, representing 19%–60% of all *UGT* mRNAs. In line with this, there are many examples in the literature of protein functional expansion created by AS, among which the human tRNA synthetases and brain neurexins are remarkable recent examples (Lo et al., 2014; Treutlein et al., 2014). Our data further indicate that UGT AS programs are constitutive in normal tissues, implying that these events are associated with normal biological processes. This observation was also validated in an independent RNA-seq dataset not captured for UGT sequences (Chhibber et al., 2016). These findings support a role for AS in controlling coordinated cellular responses induced by small molecules and exposure to xenobiotics, including drugs of various classes. Given the key role played by UGTs in cellular homeostasis by inactivation of a variety of endogenous lipophilic cellular constituents, one can envision that expression of alternative UGTs may be triggered by the cellular environment and/or stimuli such as hormones and lipids (Dates et al., 2015; Hu et al., 2014). Expression of alternative UGTs is also highly likely to be triggered by exogenous stimuli and toxic xenobiotics that are common substrates of UGTs (Hu et al., 2014). It remains unknown whether other enzymes involved in parallel cellular and drug metabolism functions diversify their expression profiles and functional complexity through splice variants. A recent study indicated that this might be the case for a vast majority (>70%) of factors in drug-related pathways, such as cytochromes P450 and other transferases (Chhibber et al., 2016). However, the regulation and functional consequences of AS events for these clinically important pharmacogenes remain undefined.

We estimate that only a small fraction of the UGT variants we quantified may undergo nonsense-mediated mRNA decay according to the 50-base pair (bp) rule (Popp and Maquat, 2013), and, therefore, most observed *UGT* transcripts likely have the potential to be translated. Multiple distinct features characterize putative UGT isoforms, including truncated substrate or co-substrate-binding domains and distinctive in-frame sequences. We provide evidence that AS may represent a potential mechanism to modify canonical UGT function and to produce alternative UGT isoforms with introduced domains and divergent functions. Our findings with the *UGT1A* and *UGT2B7* transcripts, which encode, respectively, a shorter protein with an in-frame C-terminal sequence and a longer protein with an internal peptide sequence introduced, clearly support this notion. At the transcript level, *UGT1A* and *UGT2B7* expression shows high interindividual variability in the liver and kidney. Specific antibodies raised against the peptide sequences not found in canonical UGTs or any other known proteins labeled several human tissues (IHC). Co-localization of alternate isoforms with canonical UGTs in the same cell types, such as hepatocytes, was evident even though relative abundance could not be deduced. According to functional assays in intact proliferating cells, both UGT1A1_i2 and UGT2B7_i8 lack the ability to transfer a glucuronic acid moiety to the typical substrates of the canonical enzymes and, therefore, would be enzymatically null. Alternate UGT1A_i2s contain complete binding sites for both the substrate and co-substrate and a C-terminal dilysine motif encoded by the new terminal exon, but they lack the transmembrane-binding domain, which likely affects membrane topology and conformation and, thus, UGT activity. In contrast, UGT2B7_i8 contains all UGT domains but also an internal 32-residue sequence that potentially disrupts the coordination of co-substrate-to-substrate S_N2 transfer of the glucuronic acid for typical UGT2B7 substrates, such as AZT, as observed in this study. Alternatively, this region may also potentially adapt to a different set of substrates, changing substrate specificity compared with the canonical UGT2B7 enzyme that conjugates a wide variety of lipophilic metabolites and is involved in the clearance of ~25% of common medications (Guillemette et al., 2014; Stingl et al., 2014). A larger set of substrates, as well as co-substrates such as UDP-glucose, that are metabolized by UGT2B7 in addition to UDPGA (Chau et al., 2014) needs to be tested to determine whether the alternative UGT isoforms are truly enzymatically null.

When co-expressed with UGTs in human tissues and cells, alternate UGTs either inhibited or activated cellular glucuronide formation, significantly affecting inactivation of drugs and hormones. To our knowledge, a UGT acting as an inducer/activator of the glucuronidation pathway has not been reported before.

immunogenic peptide prior to tissue labeling, demonstrating specificity of staining with anti-2B7_i8. Representative images from consecutive sections of two liver tissues are shown. BD, bile ducts; HA, hepatic arteries. Scale bars, 200 μm.

(C) Metabolic alterations associated with the expression of UGT2B7_i8. HEK293 kidney and HepG2 liver cell models (expressing endogenous UGTs, including UGT2B7) were developed. UGT2B7_i8 has an apparent molecular mass of 62 kDa, slightly larger than the UGT2B7_i1 enzyme (55 kDa), as expected, upon analysis of the microsomal fractions (20 μg) from each cell model. L, human liver microsomes, as a positive control. In situ glucuronidation activity toward the UGT2B7-specific substrate AZT is enhanced by co-expression of UGT2B7_i1 and the i8 isoform in both cell models (HEK293, n = 4 assays; HepG2, n = 3 assays; in triplicate). UGT2B7_i8 did not have glucuronidation activity with AZT as a substrate. Activity is normalized to the UGT2B7_i1 level. Data are presented as mean + SD. ***$p < 0.001$, Student's t test.

(D) Interactions between UGT2B7_i8 and i1. IP of i8 from cell lysates of HEK293 cells co-expressing UGT2B7_i1 and tagged UGT2B7_i8-V5 with anti-V5 co-purifies UGT2B7_i1.

(E) UGT2B7_i1 and i8 co-localize in the ER. Each UGT2B7 variant protein stably expressed in HEK293 cells co-localizes with the ER marker PDI. Fluorescence intensity profiles are given for cross-sections (dashed lines). Scale bars, 10 μm.

(F) Cellular metabolic profiles reveal an important modulation of levels of amino acids and nucleotides induced by UGT2B7_i8 expression in HEK293 and HepG2 cell models. Data points for which the coefficient of variation exceeded 50% were omitted for clarity. Detailed metabolomics data are given in Table S1.

(G) UGT2B7_i8 enhances adhesion but reduces the proliferation rate of HEK293 cells. Left: real-time cell adhesion was measured by electrical impedance (cell index) (n = 2 independent assays in quadruplicate; significantly different for all time points). Right: proliferation was assessed by cell counts (n = 2 independent assays in triplicate), and doubling time was determined from real-time cell index data. Data are presented as mean + SD. **$p < 0.01$, ***$p < 0.001$; Student's t test. See also Figures S3 and S4.

Previous investigations by our group and others indicate that UGTs form oligomeric complexes (Ishii et al., 2010; Operaña and Tukey, 2007; Rouleau et al., 2013). The immunofluorescence evidence of close proximity in the ER membrane and co-IP data strongly suggest that the modulatory effects of the UGT1A and UGT2B7 alternative isoforms are caused by direct protein-protein interactions with their cognate UGT enzymes, and perhaps other UGTs, leading to a mixture of active and inactive complexes (Ishii et al., 2010; Operaña and Tukey, 2007; Rouleau et al., 2013). Given the enhanced stability of at least some alternative isoforms relative to the canonical UGTs, as shown for UGT1A1_i2, the effect of alternative isoforms on cellular glucuronidation activity is likely greater than anticipated from mRNA expression levels. We suggest that AS hampers or potentiates canonical UGT functions. This likely helps to coordinate and fine-tune cellular responses to numerous endogenous and exogenous stimuli, with the potential to affect drug responses and disease development and progression, especially tumorigenesis, given the altered ratio of alternative/canonical variant expression and the large interindividual variability in their expression.

Our functional investigations of the UGT2B7_i8 variant provide further evidence that alternative isoforms have extended metabolic functions that affect global cell metabolism, suggesting that they may be part of multi-enzyme complexes of a core metabolic network. The biological relevance of a metabolic shift induced by expression of UGT2B7_i8 alone warrants further characterization, but our data also suggest that the glucuronidation pathway and primary cell metabolism (e.g., amino acids and nucleotides) are interrelated enzymatic processes. Whether dimerization/oligomerization and/or glucuronidation of alternative endogenous substrates link the biological activity of these isoforms with cell metabolism remains to be addressed. Furthermore, UGT2B7_i8 expression is functionally linked to modulation of cell adhesion and proliferation, supporting the conclusion that UGTs substantially affect multiple cellular processes.

Conclusions

This study provides a comprehensive quantitative portrait of hepatic, renal, and gastrointestinal UGT transcriptomes and reveals the abundance of alternate UGT variants, which clearly expand the UGT proteome. A first biological consequence of altering the UGT transcriptome was emphasized by the functional characterization of alternative isoforms with in-frame sequences introduced, which were found to antagonize or induce cellular glucuronidation, thus affecting the inactivation of drugs and sex hormones. This study also raises the exciting possibility that different UGTs may exhibit biological functions independent of glucuronic acid transferase activity. Alternate isoform expression induced drastic shifts in multiple metabolic pathways and modified cellular phenotypes, suggesting crosstalk between various enzymatic pathways and UGTs that could serve to maintain cellular homeostasis and increase cell fitness. The broader regulatory and functional relevance of such an extensive splicing program remains to be fully characterized. We expect that this work will enable the exploration of human UGT-mediated metabolism and its potentially extended role in health and disease.

EXPERIMENTAL PROCEDURES

RNA Samples, Sequencing, and mRNA Expression

UGT expression was characterized in normal tissue samples from nine liver, nine kidney, and 15 intestine and colon samples as well as in samples from nine kidney and nine intestine and colon tumor tissues of mixed-gender origin. For each tissue, equivalent amounts of total RNA from at least three samples were pooled, and three pools per tissue type were prepared and used for the production of sequencing libraries. UGT sequences were enriched from paired-end bar-coded cDNA libraries with UGT capture (Tourancheau et al., 2016). The libraries were sequenced on an Illumina HiSeq 2500 system (McGill University and Génome Québec Innovation Center). Trimmed reads were aligned with the splice-aware software TopHat2 on the UCSC hg19 reference genome with annotation provided by Illumina iGenome combined with the complete annotated human UGT loci described recently by our group (Tourancheau et al., 2016). The average normalized expression of replicates is provided throughout the text. Detailed library construction, sequence analysis, and validation of *UGT2B7_n4* expression by reverse transcription PCR and Sanger sequencing are described in the Supplemental Experimental Procedures.

Expression of *UGT1A* and *UGT2B7* variants was examined in 18 normal liver and 18 normal kidney samples in the RNA-seq dataset from the Pharmacogenomics Research Network (Chhibber et al., 2016) accessed from the GEO: GSE70503. Alignment of reads on the complete human UGT transcriptome and quantification using Cufflinks are described in the Supplemental Experimental Procedures.

Cell Models

HT115 cells expressing endogenous UGT1A isoforms and HEK293 cell models expressing myc- or V5-tagged UGT1A1 isoforms have been described previously (Bellemare et al., 2010a; Rouleau et al., 2014). The pool of HEK293 cells stably expressing *UGT2B7_v1* was established by supplementing cell culture media with G418 (Invitrogen, 1 mg/mL). The pool of HEK293 cells co-expressing *UGT2B7_v1* and *UGT2B7_n4* (corresponding to the exon 2b encoding transcript) was established by subsequent transfection of HEK-2B7_v1 with the UGT2B7_n4 construct (with or without a V5 tag) and selection with blasticidin (Wisent, 10 μg/mL). The HEK293 cell model expressing UGT2B7_i1 and UGT2B7_i8-V5 was used only to demonstrate protein-protein interactions by IP. HepG2 cells, which express *UGT2B7_v1* endogenously but not *UGT2B7_n4*, were transfected with the UGT2B7_n4 construct (without a tag), and the pool was established with blasticidin selection. Control HEK293 and HepG2 cells were produced by transfection with the parental vectors and selection as above.

Analysis of Protein Expression

Antibodies

The UGT2B7 polyclonal antibody was from ProteinTech Group (16661-1-AP; western blotting (WB), 1:5,000; IHC, 1:800; IF, 1:500), and the monoclonal antibody was from Abcam (ab57685; IP, 1:100; note that ab57685 is sold as an anti-UGT2B10 antibody, but it also recognizes UGT2B7 [Figure S5]). The purified pan-UGT1A polyclonal antibody (RC-71; WB, 1:1,000), purified UGT1A_i1 polyclonal antibody (9348; IHC and IF, 1:1,000; IP, 1:200), and purified UGT1A_i2 antibody (4863; IHC, 1:1,000) have been described previously (Albert et al., 1999; Bellemare et al., 2011). UGT1A_i2 (4C5E7; IF, 1:100) and UGT2B7_i8 (IF and IHC, 1:1,000) antibodies were custom made (GenScript). Anti-V5 (WB, 1:5,000) and anti-myc (clone 4A6; WB, 1:5,000) were from Invitrogen and EMD Millipore, respectively. Cell compartment-specific antibodies used in IF were as follows: anti-58K Golgi protein (1:100, ab27043, Abcam) and anti-protein disulfide isomerase (PDI) (1:100, ab2792, Abcam) for the ER and anti-cytochrome *c* (1:300, 12963S, Cell Signaling Technology) for the mitochondria. DNA was stained with Hoechst 33342 (1:1,500, Sigma) or DRAQ5 (1:2,000; Life Technologies). The production of antibodies against variants is detailed in the Supplemental Experimental Procedures.

mRNA and Protein Stability of UGT1A and UGT2B7

Cells were treated with 20 μg/mL cycloheximide for 0–16 hr and collected at various time points as described previously (Turgeon et al., 2001). Cell

homogenates (20 μg protein) prepared in PBS containing 0.5 mM DTT were analyzed by WB with RC-71 (UGT1A) or anti-UGT2B7 from ProteinTech.

IF

Detection of endogenous UGT1A_i1 and _i2 in HT115 cells was as described previously (Bellemare et al., 2010b). Stably expressed UGT2B7_i1 and UGT2B7_i8 in the HEK cell models were detected with anti-2B7 16661-1-AP.

IHC

Paraffin-embedded tissue blocks were available for individual patients. The institutional board approved the study, and written consent was given by all patients concerning the use of their tissues for research purposes. Serial sections (5 μm) were deparaffinized, rehydrated, and processed using the IDetect SuperStain horseradish peroxidase (HRP) polymer kit (Empire Genomics) with an overnight incubation of tissues at 4°C with primary antibodies. Control sections were incubated with the anti-UGT2B7_i8 preadsorbed for 3 hr at room temperature with an excess of the immunogenic peptide (2 μM) to ascertain labeling specificity.

IP

HEK293 UGT1A-tagged cell models were grown to confluency in 10-cm culture dishes, washed, scraped into 800 μL lysis buffer/dish, and immunoprecipitated as described in the Supplemental Experimental Procedures using anti-UGT1A_i1 or control rabbit immunoglobulin G (IgG). For UGT2B7_i8 IP, HEK293 cells grown in two 15-cm dishes were scraped and cross-linked with 0.125% formaldehyde for 10 min at 37°C and then quenched with 0.125 M glycine. Cells were collected by centrifugation prior to lysis in 1 mL lysis buffer and immunoprecipitated as described in the Supplemental Experimental Procedures.

MS-Coupled Multiple Reaction Monitoring

Tryptic digests of UGT2B7 immunoprecipitated from human liver S9 fractions were analyzed by MS-coupled multiple reaction monitoring on a QTRAP 6500 hybrid triple quadrupole/linear ion trap mass spectrometer (Sciex). The UGT2B7 signature peptide ADVWLIR and the UGT2B7_i8-specific peptide LDSFNTGWINK were detected in tryptic digests of the immunoprecipitated UGT2B7 samples, and peptide identity was confirmed by co-injection of isotopically labeled [^{13}C6,^{15}N2]Lys and [^{13}C6,^{15}N4]Arg synthetic peptides.

Cell Adhesion and Proliferation

HEK293 and HepG2 cells (a pool of control cells or cells stably expressing *UGT2B7_n4*) plated in E-view PET 16-well plates (10,000 cells/well, 4 replicates/experiment, n = 3) were monitored in real time on an Xcelligence DP system (ACEA Biosciences). Doubling time was determined with RTCA software 2.0 (ACEA Biosciences) using normalized cell index values between the 20- and 45-hr time points. Alternatively, HEK293 and HepG2 cells were plated in 6-well plates (125,000 HEK cells/well, 100,000 HepG2 cells/well), incubated for specified times, and counted with a TC-10 automated cell counter (Bio-Rad) 48, 72, and 96 hr after plating. Cell media were replaced after the 48-hr time point.

Metabolic Functions

In Situ Glucuronidation Assays

HEK293 and HepG2 cells (control cells or cells stably expressing *UGT2B7_v1*, *UGT2B7_n4*, or both as stated in the figure legends) were seeded in 24-well plates (HEK293, 80,000 cells/well; HepG2, 125,000 cells/well). Assays were initiated 72 hr after seeding by replacing the culture medium with fresh medium (1 mL/well) containing a labeled UGT substrate probe (for UGT1A1, 5 μM SN-38 prepared by hydrolysis of irinotecan-HCl [McKesson] and/or 25 μM estradiol [Steraloids]; for UGT2B7, AZT [Sigma-Aldrich]). Cells were incubated for 4 hr, and the media were collected and stored at −20°C until glucuronide assessment by MS-based analysis as described previously (Bélanger et al., 2009; Lépine et al., 2004). Briefly, for zidovudine-glucuronide (AZT-G), the culture media were diluted 1:3 with 25% aqueous methanol solution containing AZT-d3-G standard (Toronto Research Chemicals) prior to analysis as described previously (Bélanger et al., 2009).

Untargeted Metabolomics Analysis

HEK293 and HepG2 cells (a stable pool of control cells or cells expressing *UGT2B7_n4*) were plated in 10-cm culture dishes (1.5 million HEK cells/dish; 3.5 million HepG2 cells/dish) and grown for 96 hr with a change to fresh medium after the first 48 hr. Cells were harvested by trypsinization, counted, rinsed twice in ice-cold PBS, snap-frozen on dry ice, and stored at −80°C until extraction for metabolomics analysis. Untargeted global metabolite profiling was conducted on triplicate samples at the West Coast Metabolomics Center (University of California at Davis) as described previously (Fiehn et al., 2008). Relative quantification data provided as normalized peak heights were further normalized for cell counts in each sample and expressed as fold change ratios of mean metabolite levels in the cells expressing variant UGT2B7 versus control cells. Details about the data analysis are provided in the Supplemental Experimental Procedures.

ACCESSION NUMBERS

The accession number for the RNA sequencing data reported in this paper is GEO: GSE80463.

SUPPLEMENTAL INFORMATION

Supplemental Information includes Supplemental Experimental Procedures, five figures, and one table and can be found with this article online at http://dx.doi.org/10.1016/j.celrep.2016.08.077.

AUTHOR CONTRIBUTIONS

Conceptualization, M.R. and C.G.; Methodology, M.R. and C.G.; Investigation, M.R., A.T., C.G.B., L.V., A.M.D., Y.A.D., I.G., A.D., and C.G.; Validation, M.R., A.T., C.G.B., L.V., J.V., I.P., A.D., and C.G.; Writing – Original Draft, M.R. and C.G.; Writing – Review & Editing, M.R., A.T., C.G.B., L.V., J.V., A.M.D., Y.A.D., I.G., I.P., A.D., and C.G.; Supervision, M.R. and C.G.; Project Administration, C.G.; Funding Acquisition, C.G.

ACKNOWLEDGMENTS

We acknowledge Patrick Caron and Véronique Turcotte for their contribution to the mass spectrometry analysis of glucuronide metabolites, Sylvie Desjardins for contributing to IP experiments, Andréa Fournier for contributing to the adhesion and proliferation experiments, Joannie Roberge and Hugo Girard for contributing to the protein stability experiments, Sandra Guauque-Olarte for GEO submission of RNA sequencing data, Johanne Ouellet and Michèle Orain for contributing to the IHC analysis, Isabelle Kelly from the Proteomics platform at the CHU de Québec Research Center for support with the multiple reaction monitoring analysis, France Couture for artwork, and Dr. Éric Lévesque for helpful discussion. This work was financially supported by grants from the Canadian Institutes for Health Research (MOP-42392 and MOP-142318), the Natural Sciences and Engineering Research Council of Canada (342176-2012), and a Canadian Research Chair in Pharmacogenomics (to C.G., Tier I). C.G.B. holds an FER studentship award from the Faculty of Pharmacy of Laval University. Y.A.D. received studentship funding from the Centre de Recherche en Endocrinologie Moléculaire et Oncologique et Génomique Humaine, Laval University and Fonds de Recherche du Québec – Santé. C.G. holds the Canada Research Chair in Pharmacogenomics.

Received: April 22, 2016
Revised: July 15, 2016
Accepted: August 23, 2016
Published: September 27, 2016

REFERENCES

Albert, C., Vallée, M., Beaudry, G., Bélanger, A., and Hum, D.W. (1999). The monkey and human uridine diphosphate-glucuronosyltransferase UGT1A9, expressed in steroid target tissues, are estrogen-conjugating enzymes. Endocrinology *140*, 3292–3302.

Bélanger, A.S., Caron, P., Harvey, M., Zimmerman, P.A., Mehlotra, R.K., and Guillemette, C. (2009). Glucuronidation of the antiretroviral drug efavirenz by UGT2B7 and an in vitro investigation of drug-drug interaction with zidovudine. Drug Metab. Dispos. *37*, 1793–1796.

Bellemare, J., Rouleau, M., Harvey, M., and Guillemette, C. (2010a). Modulation of the human glucuronosyltransferase UGT1A pathway by splice isoform polypeptides is mediated through protein-protein interactions. J. Biol. Chem. *285*, 3600–3607.

Bellemare, J., Rouleau, M., Harvey, M., Têtu, B., and Guillemette, C. (2010b). Alternative-splicing forms of the major phase II conjugating UGT1A gene negatively regulate glucuronidation in human carcinoma cell lines. Pharmacogenomics J. *10*, 431–441.

Bellemare, J., Rouleau, M., Harvey, M., Popa, I., Pelletier, G., Têtu, B., and Guillemette, C. (2011). Immunohistochemical expression of conjugating UGT1A-derived isoforms in normal and tumoral drug-metabolizing tissues in humans. J. Pathol. *223*, 425–435.

Bock, K.W. (2015). Roles of human UDP-glucuronosyltransferases in clearance and homeostasis of endogenous substrates, and functional implications. Biochem. Pharmacol. *96*, 77–82.

Breton, C., Fournel-Gigleux, S., and Palcic, M.M. (2012). Recent structures, evolution and mechanisms of glycosyltransferases. Curr. Opin. Struct. Biol. *22*, 540–549.

Chau, N., Elliot, D.J., Lewis, B.C., Burns, K., Johnston, M.R., Mackenzie, P.I., and Miners, J.O. (2014). Morphine glucuronidation and glucosidation represent complementary metabolic pathways that are both catalyzed by UDP-glucuronosyltransferase 2B7: kinetic, inhibition, and molecular modeling studies. J. Pharmacol. Exp. Ther. *349*, 126–137.

Chhibber, A., French, C.E., Yee, S.W., Gamazon, E.R., Theusch, E., Qin, X., Webb, A., Papp, A.C., Wang, A., Simmons, C.Q., et al. (2016). Transcriptomic variation of pharmacogenes in multiple human tissues and lymphoblastoid cell lines. Pharmacogenomics J. Published online February 9, 2016. http://dx.doi.org/10.1038/tpj.2015.93.

Clark, M.B., Mercer, T.R., Bussotti, G., Leonardi, T., Haynes, K.R., Crawford, J., Brunck, M.E., Cao, K.A., Thomas, G.P., Chen, W.Y., et al. (2015). Quantitative gene profiling of long noncoding RNAs with targeted RNA sequencing. Nat. Methods *12*, 339–342.

Court, M.H., Zhang, X., Ding, X., Yee, K.K., Hesse, L.M., and Finel, M. (2012). Quantitative distribution of mRNAs encoding the 19 human UDP-glucuronosyltransferase enzymes in 26 adult and 3 fetal tissues. Xenobiotica *42*, 266–277.

Dates, C.R., Fahmi, T., Pyrek, S.J., Yao-Borengasser, A., Borowa-Mazgaj, B., Bratton, S.M., Kadlubar, S.A., Mackenzie, P.I., Haun, R.S., and Radominska-Pandya, A. (2015). Human UDP-Glucuronosyltransferases: Effects of altered expression in breast and pancreatic cancer cell lines. Cancer Biol. Ther. *16*, 714–723.

De Bruyn, F., Maertens, J., Beauprez, J., Soetaert, W., and De Mey, M. (2015). Biotechnological advances in UDP-sugar based glycosylation of small molecules. Biotechnol. Adv. *33*, 288–302.

Fiehn, O., Wohlgemuth, G., Scholz, M., Kind, T., Lee, D.Y., Lu, Y., Moon, S., and Nikolau, B. (2008). Quality control for plant metabolomics: reporting MSI-compliant studies. Plant J. *53*, 691–704.

Gamazon, E.R., and Stranger, B.E. (2014). Genomics of alternative splicing: evolution, development and pathophysiology. Hum. Genet. *133*, 679–687.

Garcia-Blanco, M.A., Baraniak, A.P., and Lasda, E.L. (2004). Alternative splicing in disease and therapy. Nat. Biotechnol. *22*, 535–546.

Guillemette, C. (2003). Pharmacogenomics of human UDP-glucuronosyltransferase enzymes. Pharmacogenomics J. *3*, 136–158.

Guillemette, C., Bélanger, A., and Lépine, J. (2004). Metabolic inactivation of estrogens in breast tissue by UDP-glucuronosyltransferase enzymes: an overview. Breast Cancer Res. *6*, 246–254.

Guillemette, C., Lévesque, É., and Rouleau, M. (2014). Pharmacogenomics of human uridine diphospho-glucuronosyltransferases and clinical implications. Clin. Pharmacol. Ther. *96*, 324–339.

Hu, D.G., Meech, R., McKinnon, R.A., and Mackenzie, P.I. (2014). Transcriptional regulation of human UDP-glucuronosyltransferase genes. Drug Metab. Rev. *46*, 421–458.

Ishii, Y., Takeda, S., and Yamada, H. (2010). Modulation of UDP-glucuronosyltransferase activity by protein-protein association. Drug Metab. Rev. *42*, 145–158.

Lépine, J., Bernard, O., Plante, M., Têtu, B., Pelletier, G., Labrie, F., Bélanger, A., and Guillemette, C. (2004). Specificity and regioselectivity of the conjugation of estradiol, estrone, and their catecholestrogen and methoxyestrogen metabolites by human uridine diphospho-glucuronosyltransferases expressed in endometrium. J. Clin. Endocrinol. Metab. *89*, 5222–5232.

Little, J.M., Kurkela, M., Sonka, J., Jäntti, S., Ketola, R., Bratton, S., Finel, M., and Radominska-Pandya, A. (2004). Glucuronidation of oxidized fatty acids and prostaglandins B1 and E2 by human hepatic and recombinant UDP-glucuronosyltransferases. J. Lipid Res. *45*, 1694–1703.

Lo, W.S., Gardiner, E., Xu, Z., Lau, C.F., Wang, F., Zhou, J.J., Mendlein, J.D., Nangle, L.A., Chiang, K.P., Yang, X.L., et al. (2014). Human tRNA synthetase catalytic nulls with diverse functions. Science *345*, 328–332.

Mackenzie, P.I., Bock, K.W., Burchell, B., Guillemette, C., Ikushiro, S., Iyanagi, T., Miners, J.O., Owens, I.S., and Nebert, D.W. (2005). Nomenclature update for the mammalian UDP glycosyltransferase (UGT) gene superfamily. Pharmacogenet. Genomics *15*, 677–685.

Margaillan, G., Rouleau, M., Fallon, J.K., Caron, P., Villeneuve, L., Turcotte, V., Smith, P.C., Joy, M.S., and Guillemette, C. (2015a). Quantitative profiling of human renal UDP-glucuronosyltransferases and glucuronidation activity: a comparison of normal and tumoral kidney tissues. Drug Metab. Dispos. *43*, 611–619.

Margaillan, G., Rouleau, M., Klein, K., Fallon, J.K., Caron, P., Villeneuve, L., Smith, P.C., Zanger, U.M., and Guillemette, C. (2015b). Multiplexed Targeted Quantitative Proteomics Predicts Hepatic Glucuronidation Potential. Drug Metab. Dispos. *43*, 1331–1335.

Mercer, T.R., Gerhardt, D.J., Dinger, M.E., Crawford, J., Trapnell, C., Jeddeloh, J.A., Mattick, J.S., and Rinn, J.L. (2011). Targeted RNA sequencing reveals the deep complexity of the human transcriptome. Nat. Biotechnol. *30*, 99–104.

Oltean, S., and Bates, D.O. (2014). Hallmarks of alternative splicing in cancer. Oncogene *33*, 5311–5318.

Operaña, T.N., and Tukey, R.H. (2007). Oligomerization of the UDP-glucuronosyltransferase 1A proteins: homo- and heterodimerization analysis by fluorescence resonance energy transfer and co-immunoprecipitation. J. Biol. Chem. *282*, 4821–4829.

Popp, M.W., and Maquat, L.E. (2013). Organizing principles of mammalian nonsense-mediated mRNA decay. Annu. Rev. Genet. *47*, 139–165.

Radominska-Pandya, A., Czernik, P.J., Little, J.M., Battaglia, E., and Mackenzie, P.I. (1999). Structural and functional studies of UDP-glucuronosyltransferases. Drug Metab. Rev. *31*, 817–899.

Rouleau, M., Collin, P., Bellemare, J., Harvey, M., and Guillemette, C. (2013). Protein-protein interactions between the bilirubin-conjugating UDP-glucuronosyltransferase UGT1A1 and its shorter isoform 2 regulatory partner derived from alternative splicing. Biochem. J. *450*, 107–114.

Rouleau, M., Roberge, J., Bellemare, J., and Guillemette, C. (2014). Dual roles for splice variants of the glucuronidation pathway as regulators of cellular metabolism. Mol. Pharmacol. *85*, 29–36.

Rowland, A., Miners, J.O., and Mackenzie, P.I. (2013). The UDP-glucuronosyltransferases: their role in drug metabolism and detoxification. Int. J. Biochem. Cell Biol. *45*, 1121–1132.

Stingl, J.C., Bartels, H., Viviani, R., Lehmann, M.L., and Brockmöller, J. (2014). Relevance of UDP-glucuronosyltransferase polymorphisms for drug dosing: A quantitative systematic review. Pharmacol. Ther. *141*, 92–116.

Tourancheau, A., Margaillan, G., Rouleau, M., Gilbert, I., Villeneuve, L., Lévesque, E., Droit, A., and Guillemette, C. (2016). Unravelling the transcriptomic landscape of the major phase II UDP-glucuronosyltransferase drug metabolizing pathway using targeted RNA sequencing. Pharmacogenomics J. *16*, 60–70.

Treutlein, B., Gokce, O., Quake, S.R., and Südhof, T.C. (2014). Cartography of neurexin alternative splicing mapped by single-molecule long-read mRNA sequencing. Proc. Natl. Acad. Sci. USA *111*, E1291–E1299.

Turgeon, D., Carrier, J.S., Lévesque, E., Hum, D.W., and Bélanger, A. (2001). Relative enzymatic activity, protein stability, and tissue distribution of human steroid-metabolizing UGT2B subfamily members. Endocrinology *142*, 778–787.

Wang, E.T., Sandberg, R., Luo, S., Khrebtukova, I., Zhang, L., Mayr, C., Kingsmore, S.F., Schroth, G.P., and Burge, C.B. (2008). Alternative isoform regulation in human tissue transcriptomes. Nature *456*, 470–476.

Wells, P.G., Mackenzie, P.I., Chowdhury, J.R., Guillemette, C., Gregory, P.A., Ishii, Y., Hansen, A.J., Kessler, F.K., Kim, P.M., Chowdhury, N.R., and Ritter, J.K. (2004). Glucuronidation and the UDP-glucuronosyltransferases in health and disease. Drug Metab. Dispos. *32*, 281–290.